JOURNAL OF SYNCHROTRON RADIATION
ISSN 1600-5775

Enhanced insulating behavior in the Ir-vacant $Sr_2Ir_{1-x}O_4$ system dominated by the local structure distortion

Jie Cheng,[a]* Peng Dong,[b] Bin Li,[a] Shengli Liu,[a,c]* Xiangfu Wang,[b] Yu Wang[d] and Xing'ao Li[a]

[a]New Energy Technology Engineering Laboratory of Jiangsu Province, School of Science, Nanjing University of Posts and Telecommunications, Nanjing, Jiangsu 210023, People's Republic of China, [b]College of Electronic and Optical Engineering, Nanjing University of Posts and Telecommunications, Nanjing, Jiangsu 210023, People's Republic of China, [c]Nanjing University (Suzhou) High-Tech Institute, Suzhou 215123, People's Republic of China, and [d]Shanghai Synchrotron Radiation Facility, Shanghai Institute of Applied Physics, Chinese Academy of Sciences, Shanghai 201204, People's Republic of China. *Correspondence e-mail: chengj@njupt.edu.cn, liusl@njupt.edu.cn

Received 20 January 2018
Accepted 13 April 2018

Edited by R. W. Strange, University of Essex, UK

Keywords: $Sr_2Ir_{1-x}O_4$; X-ray absorption spectroscopy; local structure distortion.

Sr_2IrO_4, known as the J_{eff} = 1/2 Mott insulator, was predicted to be an unconventional superconductor upon doping since it highly resembles the high-temperature cuprates. However, recent work pointed out an enhanced insulating behavior in the Ir-vacant $Sr_2Ir_{1-x}O_4$ system. In this contribution, to investigate the microscopic mechanism of its enhanced insulating behavior, X-ray absorption spectroscopy was applied to study the electronic structure and local structure distortion of $Sr_2Ir_{1-x}O_4$. Due to the presence of Ir^{5+} ions, the preconceived holes are barely doped in the Ir-vacant system. Nevertheless, Ir vacancies finely modulate the local atomic structure, *i.e.* the topology of IrO_6 octahedra and the in-plane Ir—O1—Ir bond angle. Combined with theoretical calculations, it is demonstrated that both the more distorted IrO_6 octahedra and decreased Ir—O1—Ir angle contribute to the increment of the band gap, and then result in the enhanced insulating state for $Sr_2Ir_{1-x}O_4$.

1. Introduction

The 5*d* transition metal oxides (TMOs) have received substantial attention in recent times due to their numerous intriguing phenomena, such as the J_{eff} = 1/2 Mott insulator (Kim *et al.*, 2008, 2009), a giant magnetoelectric effect (Chikara *et al.*, 2009), Weyl semi-metals (Witczak-Krempa *et al.*, 2014), *etc*. In particular, the spin–orbit coupling (SOC) is an important factor in governing their unusual properties. The electron–electron interaction becomes weaker, while the SOC ranges from 0.4 to 1 eV in 5*d* materials, which is much larger than those of 3*d*/4*d* TMOs. The SOC vigorously competes with on-site Coulomb (0.5–2 eV) and other fundamental interactions, therefore, a new balance between the relevant energies is established and could give rise to some interesting properties of 5*d* TMOs.

Sr_2IrO_4, with a crystal structure similar to that of La_2CuO_4 (Kim *et al.*, 2012), is an interesting member of the 5*d* TMOs. A unique and important structural feature of Sr_2IrO_4 is that it crystallizes in a reduced tetragonal structure with an $I4_1/acd$ space group where the IrO_6 octahedra exhibit a rotation of about 11° around the *c*-axis (Crawford *et al.*, 1994). This rotation corresponds to a distorted in-plane Ir—O—Ir bond angle that is critical to the electronic structure (Ge *et al.*, 2011). Moreover, the rotation is believed to bring in a Dzyaloshinsky–Moriya interaction which leads to a transition to a

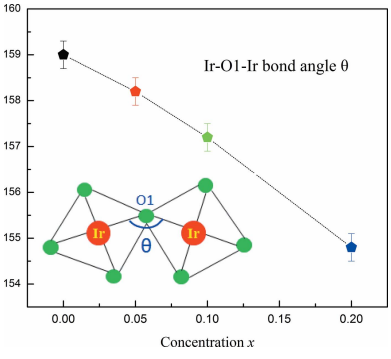

weak ferromagnetic phase with a transition temperature of ~240 K (Crawford *et al.*, 1994). On the other hand, the 5*d* orbitals are spatially more extended than 3*d*/4*d* orbitals, and their Coulomb interactions could be smaller than those of 3*d*/4*d* orbitals. Thus 5*d* TMOs are expected to have a metallic ground state. Contrary to the conventional understanding of the electron correlation, it is already established that Sr_2IrO_4 is a unique $J_{\rm eff} = 1/2$ Mott insulator dictated by the cooperation of the SOC and on-site Coulomb interaction (Kim *et al.*, 2008).

The Sr_2IrO_4-based system has been predicted to be a new kind of high-temperature superconductor (Watanabe *et al.*, 2013; Meng *et al.*, 2014; Yang *et al.*, 2014), inspired by the structurally and electronically analogous La_2CuO_4 (Bednorz & Müller, 1986) and the *p*-wave superconductor Sr_2RuO_4 (Nelson *et al.*, 2004). Recent angle-resolved photoemission spectroscopy (ARPES) has shown a predominant *d*-wave gap in electron-doped Sr_2IrO_4 (Kim *et al.*, 2016), and a closed pseudogap at about 50 K is further detected by scanning tunneling microscopy/spectroscopy (STM/STS) of Sr_2IrO_4 with surface potassium coverage (Yan *et al.*, 2015), which, however, needs more supporting material. In order to achieve bulk superconductivity, many experimental studies have been carried out through a variety of means; these include electron doping (*e.g.* La substitution; Klein & Terasaki, 2008) and hole-doping (*e.g.* substitution of Rh for Ir; Chikara *et al.*, 2017). Although superconductivity has not been discovered, the element substitution suppresses the magnetism and strongly affects transport.

In addition, vacancies are also an effective way for carrier doping, which could also induce novel physics. The typical example is oxygen vacancies in Sr_2IrO_{4-x}. Dilute oxygen vacancies with $x \leq 0.04$ leads to significant changes in lattice parameters and an insulator-to-metal transition at 105 K (Korneta *et al.*, 2010). Moreover, a study in deep Sr-vacant $Sr_{2-x}IrO_4$ observed significant structural changes around $x \simeq 0.48$ in both lattice constants and Ir—O bond length, accompanied by an insulator–metal transition (Sun *et al.*, 2016). Very recently, an enhanced insulating state was observed in Ir-vacant $Sr_2Ir_{1-x}O_4$ compounds (Yu *et al.*, 2017), which is surprising because Ir-vacancies are supposed to dope holes into the system, and most other doping/vacancies lead to the conductive state. Hence, it is interesting and urgent to investigate the microscopic mechanism of the enhanced insulating behavior in the $Sr_2Ir_{1-x}O_4$ system.

As is well known, material properties are closely related to their local atomic structures. Previous studies have demonstrated that doping/vacancies could modulate the lattice parameters and further change the electronic and magnetic behaviors of the Sr_2IrO_4 system (Kong *et al.*, 2015; Sun *et al.*, 2016). Therefore, the most important issue to be resolved for Ir-vacant $Sr_2Ir_{1-x}O_4$ is how Ir-vacancies affect the physical properties in terms of local atomic structure. Synchrotron-radiation-based X-ray absorption spectroscopy (XAS), consisting of X-ray absorption near-edge spectroscopy (XANES) and extended X-ray absorption fine-structure (EXAFS), is an ideal technique for retrieving substantial information (*i.e.* nanoscale atomic displacements and local electronic structure), and thus XAS has been widely applied in Sr_2IrO_4-based systems. For example, Ir $L_{2,3}$-edge XAS pointed out the synergistic effect of regular IrO_6 octahedra and electron doping that accounts for the transition from a Mott insulator to a conductive state in $Sr_{2-x}La_xIrO_4$ compounds (Cheng *et al.*, 2016). Moreover, the critical point ($x \simeq 0.48$) in $Sr_{2-x}IrO_4$ is due to the less distorted IrO_6 octahedra induced by deep Sr-vacancies (Cheng *et al.*, 2017). In this contribution, we take the polycrystalline compounds $Sr_2Ir_{1-x}O_4$ as the object of our research, and report a detailed investigation of the Ir-vacancy effect, through a comprehensive analysis of Ir $L_{2,3}$-edge XAS.

2. Experiments and calculations

Polycrystalline compounds of $Sr_2Ir_{1-x}O_4$ ($x = 0, 0.05, 0.10, 0.20$) were synthesized through the conventional solid-state reaction method as mentioned elsewhere (Yu *et al.*, 2017). The samples were well characterized for their phase purity, transport and magnetic properties prior to the XAS measurements (Yu *et al.*, 2017). We collected Ir L_2-edge XANES and L_3-edge EXAFS spectra of $Sr_2Ir_{1-x}O_4$ at room temperature, which occur at energies of 12.824 keV and 11.215 keV, respectively. XAS measurements were performed in transmission mode at the BL-14W1 beamline of Shanghai Synchrotron Radiation Facility. Several scans were collected to ensure the spectral reproducibility. The storage ring was working at an electron energy of 3.5 GeV, and the maximum stored current was about 250 mA. Data were recorded using a Si(111) double-crystal monochromator and normalized by the *IFEFFIT* program package (Newville, 2001).

The density functional theory (DFT) code *OPENMX* was used for the theoretical calculation on the electronic structure. The calculation is based on a linear-combination-of-pseudo-atomic-orbitals (LCPAO) method (Ozaki, 2003), whereby the local density approximation + *U* method and SOC (LDA + *U* + SOC) are included *via* a fully relativistic *j*-dependent pseudopotential in the non-collinear DFT scheme.

3. Results and discussion

If the ionic oxidation state of Ir remains unchanged, Ir-vacancies would introduce holes into the system, and then contribute to the conductive state, which is inconsistent with an enhanced insulating behavior in $Sr_2Ir_{1-x}O_4$. To clarify this puzzle, the normalized XANES spectra at the Ir $L_{2,3}$-edge for $Sr_2Ir_{1-x}O_4$ compounds are displayed in Fig. 1. The most striking characteristics at both L_2- and L_3-edges are the prominent white-line (WL) features, which correspond to the electronic transition from 2*p* to unoccupied 5*d* states. The branching ratio BR = I_{L3}/I_{L2}, where $I_{L2,3}$ is the integrated WL intensity at the L_2- and L_3-edges (Clancy *et al.*, 2012), is close to 6.5 for all the Ir-vacant samples. This differs significantly from the statistical branching ratio of 2, indicating the presence of extremely large SOC effects in the Sr_2IrO_4-based system. Furthermore, the WL intensity is proportional to the local density of unoccupied final states (*i.e.* the population of

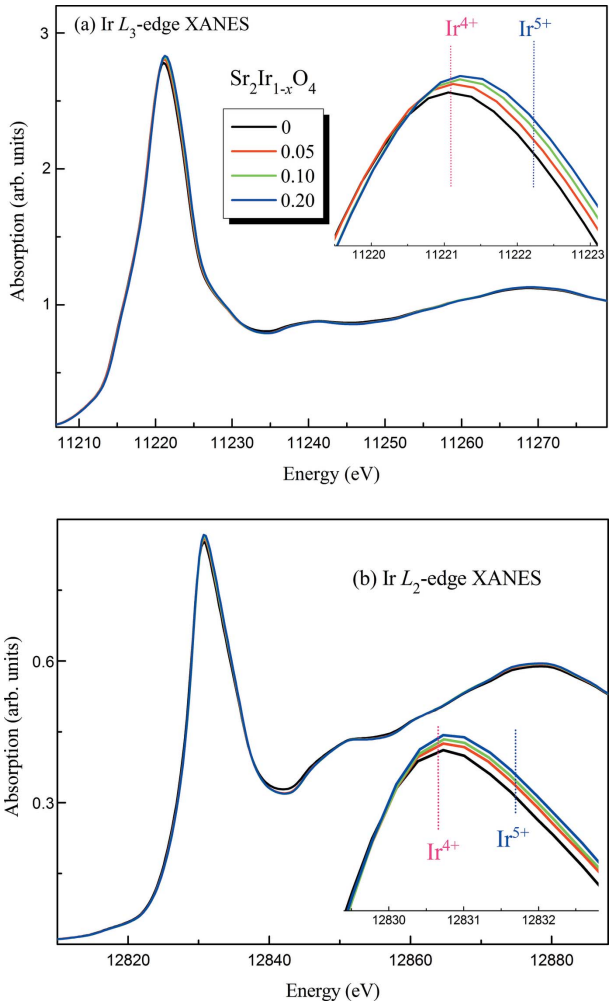

Figure 1
Ir $L_{2,3}$-edge XANES spectra for $Sr_2Ir_{1-x}O_4$. A magnified view of the white-line peak is shown in the inset.

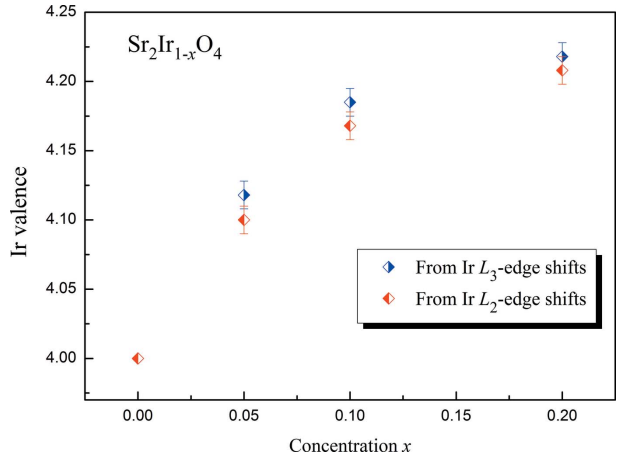

Figure 2
The valence state of Ir as a function of Ir-vacancies, obtained from Ir $L_{2,3}$-edge shifts.

5*d* holes). From Fig. 1 the intensity of the WL features at both absorption edges grows steadily with increasing Ir-vacancies, suggesting an increment of Ir-5*d* holes in the $Sr_2Ir_{1-x}O_4$ system. Furthermore, we observed a broadening of the WL peak and a positive shift in spectral weight with increasing Ir-vacancies. Both of these features indicate a mixed population of Ir^{4+} and Ir^{5+} ions introduced by Ir-vacancies, consistent with the result of previous X-ray photoelectron spectroscopy (Yu *et al.*, 2017).

The Ir valence for $Sr_2Ir_{1-x}O_4$ in Fig. 2 is calculated using a linear interpolation based on the energy shift per Ir unit charge (1.24 ± 0.02 eV for the L_3-edge and 1.12 ± 0.02 eV for the L_2-edge, seen in Fig. 1) (Chikara *et al.*, 2017). Here, the fraction of Ir^{5+} ions are determined by the function $(1 - y) \times E_{Ir}{}^{4+} + y \times E_{Ir}{}^{5+} = E_{exp}$, where y is the fraction of Ir^{5+} ions, $E_{Ir}{}^{4+}$ and $E_{Ir}{}^{5+}$ are the corresponding absorption-edge energies for Ir^{4+} and Ir^{5+} ions, and E_{exp} is the experimental energy for Ir-vacant samples. Then we can obtain the mean valence of Ir in Ir-vacant samples by $v = (1 - y) \times (+4) + y \times (+5)$. Obviously, results from independent measurements at the Ir $L_{2,3}$-edges are in good agreement. Due to the presence of Ir^{5+} ions, the mean valence of Ir in all Ir-vacant samples is larger than 4+. With increasing Ir-vacancies, the fraction of Ir^{5+} ions is accordingly increased, and for $x = 0.20$ the Ir^{5+} ion is up to 22% for the $Sr_2Ir_{1-x}O_4$ system. That is to say, some Ir ions turn to a 5+ valence state to achieve charge neutrality; therefore, holes are barely doped into the $Sr_2Ir_{1-x}O_4$ system. To investigate the underlying mechanism of the enhanced insulating state, we will resort to the local atomic structure, much more sensitive to the Ir-vacancies.

First of all, the local structure changes by Ir-vacancies could be observed in the Ir $L_{2,3}$-edges XANES. But in Fig. 1 we found that the changes in the resonance peaks for Ir-vacant samples are not obvious due to the prominent WL features. Furthermore, the resonance peaks are associated with the multiple scattering, and it is difficult to provide quantitative information about the local structure changes. Consequently, the following discussions of the Ir-vacancy effect on the local structure would resort to EXAFS. Fig. 3(*a*) shows the EXAFS oscillations as a function of wavevector k, extracted from Ir L_3-edge XAS of $Sr_2Ir_{1-x}O_4$. The EXAFS are multiplied by k^3 to amplify the high k-range of the oscillations. The EXAFS oscillations are visible up to a k-value of ∼15 $Å^{-1}$ out of the noise level. The Ir-vacancies effect can be better seen in the Fourier transform (FT) magnitudes of the EXAFS oscillations providing real space information (Fig. 3*b*). The FTs are performed using a Hanning window with the k range being 3–15 $Å^{-1}$. Ir L_3-edge FTs provide the average information on the atomic distribution around the photo-absorbing Ir atoms. For the Sr_2IrO_4-based system, the IrO_6 octahedron contains two distinct oxygen positions (four basal O1 and two apical O2), which is slightly elongated apically (Crawford *et al.*, 1994). Thus the first peak of EXAFS spectra (R = 1.4–2.6 Å) corresponds to the superposition of Ir–O1 and Ir–O2 pairs. Obviously, with Ir-vacancies large changes in the first peak can be seen, indicating the effective modulation of Ir—O bonds in Ir-vacant compounds.

To determine the local structure parameters, the EXAFS amplitudes were modeled by the following general equation

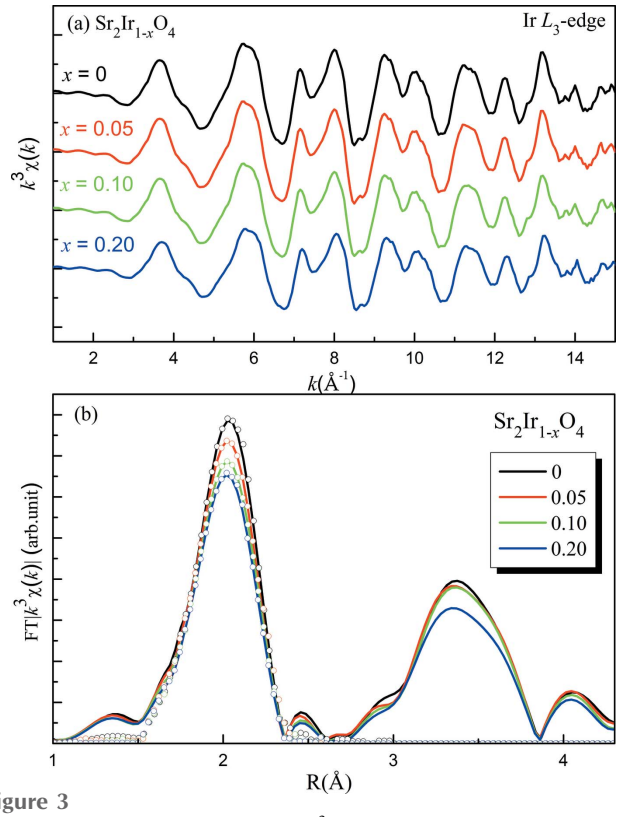

Figure 3
EXAFS oscillations (weighted by k^3) and FT magnitudes of the Ir L_3-edge EXAFS measured on $Sr_2Ir_{1-x}O_4$. The model fits to the FTs are also shown as open circles.

based on the single-scattering approximation (Rehr & Albers, 2000),

$$\chi(k) = \sum_j \frac{N_j S_0^2}{kR_j^2} f_j(k, R_j) \times \exp\left(-2k^2\sigma_j^2\right) \exp\left(-2R_j/\lambda\right) \times \sin\left[2kR_j + \delta_j(k)\right], \quad (1)$$

where N_j is the number of neighboring atoms at a distance R_j from the photo-absorbing atom, S_0^2 is the so-called passive electron reduction factor, $f_j(k, R_j)$ is the backscattering amplitude, λ is the photoelectron mean free path, $\delta_j(k)$ is the phase shift and σ_j^2 is the correlated Debye–Waller factor.

For the least-squares fits, the average structure parameter obtained by diffraction on Sr_2IrO_4 was used as the starting model (Yu *et al.*, 2017). Model fits of two shells, involving contributions from four Ir—O1 and two Ir—O2 bond distances, were performed to fit the first peak in FTs using the *Artemis* software (Newville, 2001). The backscattering amplitudes and phase shift were calculated using the *FEFF* code (Ankudinov *et al.*, 1998). Only the radial distances R_j and the corresponding σ_j^2 were allowed to vary in the least-squares fits, with coordination numbers N_j fixed to the nominal values. The passive electrons reduction factor S_0^2 and photoelectron energy zero E_0 were also fixed after fit trials on different scans. The number of independent parameters which could be determined by EXAFS is limited by the number of the independent data points $N_{\rm ind} \simeq (2\Delta k\Delta R)/\pi$, where Δk and ΔR are the ranges of the fit in the k and R space, respectively. In our case, $N_{\rm ind}$ is 9 ($\Delta k = 12$ Å^{-1}, $\Delta R = 1.2$ Å), sufficient to obtain all parameters. The spatial resolution to distinguish contributions from two Ir—O distances is about $\pi/2k_{\rm max} = 0.10$ Å. The model fits are also shown in Fig. 3(*b*). The *R*-factors for the EXAFS fits were found to be between 10–15% for all the samples, indicating very good fits.

Fig. 4 shows the Ir—O1/O2 bond distances and Debye–Waller factors for Ir-vacant samples. Thereinto, the errors given are statistical only, and are defined as the standard deviation of the results obtained from repeated measurements under identical conditions (Granado *et al.*, 2011). As shown in Fig. 4(*a*), the bond distances of both Ir—O1 and Ir—O2 pairs decrease gradually with increasing Ir-vacancies, generally in line with the result of pervious diffraction measurements (Yu *et al.*, 2017). Furthermore, Ir-vacancies make a significant contribution to increase the ratio of apical Ir—O2 to basal Ir—O1 distance (illustrated in Fig. 4*b*), indicating more distorted IrO_6 octahedra induced by Ir-vacancies. Previous DFT calculations have demonstrated that distorted IrO_6 octahedra lead to an increased band gap between upper Hubbard bands (UHB) and lower Hubbard bands (LHB) (Cheng *et al.*, 2016).

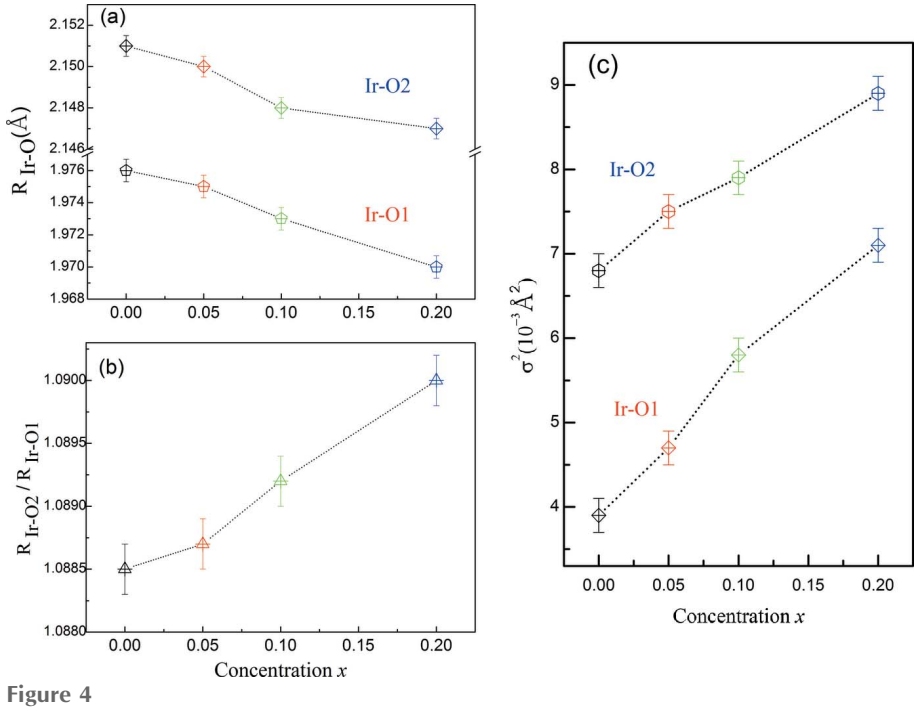

Figure 4
(*a*) Ir—O1/O2 bond distances as a function of Ir-vacant concentration x. (*b*) The ratio of apical Ir—O2 to basal Ir—O1 bond distance. (*c*) Debye–Waller factor of Ir—O1/O2 pairs as a function of Ir-vacant concentration x.

Therefore, it is assured that the enhanced insulating behavior of $Sr_2Ir_{1-x}O_4$ is partially attributed to the distorted IrO_6 octahedra. Further information on the atomic displacements is provided by the correlated Debye–Waller factor σ_j^2, measuring the mean square relative displacement of the pair of atoms (photoabsorber–backscatter pairs). The σ_j^2 values, obtained from the best fits, are shown in Fig. 4(*c*) as a function of the Ir-vacant concentration. With Ir-vacancies, the σ_j^2 values for both Ir—O1 and Ir—O2 pairs tend to increase, indicating a large configurational disorder in Ir-vacant compounds.

The electronic structure of layered perovskite is controlled by the in-plane metal–oxygen–metal bond angle, that is, the rotation of the metal–oxygen octahedral about the *c*-axis (Nakatsuji & Maeno, 2000). For Sr_2IrO_4, the IrO_6 octahedra exhibit a rotation of about 11° around the *c*-axis, which corresponds to a distorted in-plane Ir—O1—Ir bond angle θ. Previous studies of Sr_2IrO_4 have already established that the Ir—O1—Ir bond angle θ is believed to be the key structural parameter, and the electronic structure can be readily changed *via* slight manipulations of θ (Korneta *et al.*, 2010). For example, in $Sr_{1.5}IrO_4$ the insulator–metal transition is closely related to the increased in-plane Ir—O1—Ir bond angle (Sun *et al.*, 2016). Therefore, it is interesting and necessary to evaluate θ as a function of Ir-vacancies. For the previous reports, the Ir—O1—Ir angle was obtained by the refinement treatment of XRD patterns (Kong *et al.*, 2015; Yu *et al.*, 2017). It should be noted that the XRD technique can only provide an average long-range-order parameter, while no detailed local information (*e.g.* vacancy, local structural distortion) can be obtained. Fortunately, EXAFS is a unique element-selective technique and it is always used to probe the local information. Therefore, we can provide information about the Ir—O1—Ir bond angle with the use of EXAFS.

Using the bond distance measured by EXAFS and *a*-axis lattice parameter by X-ray diffraction data, we can calculate the in-plane Ir—O1—Ir angle by the formula

$$\theta = 2\arcsin\left(\frac{R_{\mathrm{Ir-Ir}}/2}{R_{\mathrm{Ir-O1}}}\right) = 2\arcsin\left(\frac{\sqrt{2}a}{2R_{\mathrm{Ir-O1}}}\right), \qquad (2)$$

where $R_{\mathrm{Ir-Ir}}$ is approximately equal to $\sqrt{2}a$. As shown in Fig. 5, we found that the Ir—O1—Ir angle θ at $x = 0$ is 159.0 (3)°, suggesting a rotation of IrO_6 octahedra. Then it decreases with Ir-vacancies, whereas θ at $x = 0.20$ is 154.8 (3)°. It is recognized that the larger the value of θ, the more energetically favorable it is for electron hopping (Ge *et al.*, 2011; Cao *et al.*, 2018). Accordingly, in our Ir-vacant system the decrease in θ would drastically weaken the electron hopping, which could explain the enhanced insulating state in $Sr_2Ir_{1-x}O_4$.

To simulate the electronic structure changes as a function of Ir—O1—Ir angle θ, we performed DFT calculations and gradually decreased the angle from 160° to 150°. It should be noted that SOC is recognized as the essential element in the calculation for the Sr_2IrO_4 system, and the previous report emphasized that the full LDA + U + SOC calculation can lead to the J_{eff} = 1/2 Mott state for Sr_2IrO_4 (Kim *et al.*, 2008). Therefore, in our calculations local density approximation + U method and SOC (LDA + U + SOC) are included. The corresponding total density of states (DOS) between −2.0 and 2.0 eV is displayed in Fig. 6, where the Ir 5*d* t_{2g} orbital states are the main contributors. The DOS above the Fermi energy corresponds to the UHB of the J_{eff} = 1/2 states. The DOS between −2.0 and −0.5 eV is from the J_{eff} = 3/2 bands, and that between −0.5 and 0.0 eV is from the LHB of the J_{eff} = 1/2 states. As the Ir—O1—Ir angle decreases from 160° to 150°, the DOS of the J_{eff} = 3/2 bands increases and that of the LHB of J_{eff} = 1/2 bands decreases, indicating a DOS redistribution between the two bands. At the same time, the band gap between the LHB and UHB of the J_{eff} = 1/2 states increases. Therefore, the DFT calculations demonstrate again the intimate relationship between the decreased Ir—O1—Ir angle θ and the enhanced insulating behavior of the Ir-vacant system.

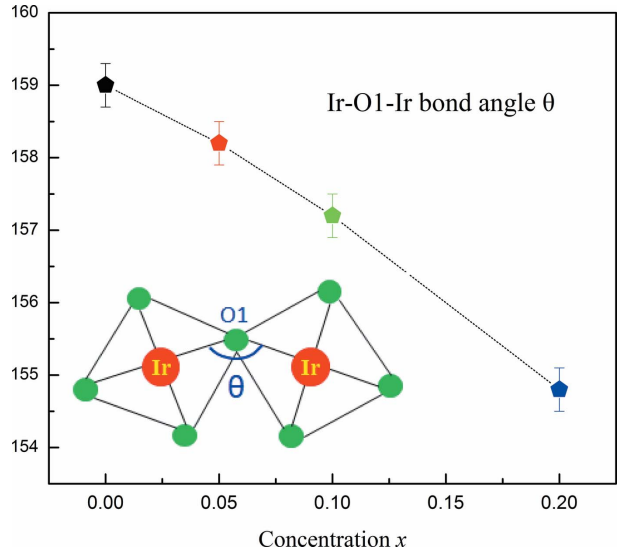

Figure 5
The Ir—O1—Ir bond angle θ as a function of Ir-vacancies. The inset shows the rotation of the two neighboring octahedra. The large red and small green circles represent Ir and O atoms, respectively.

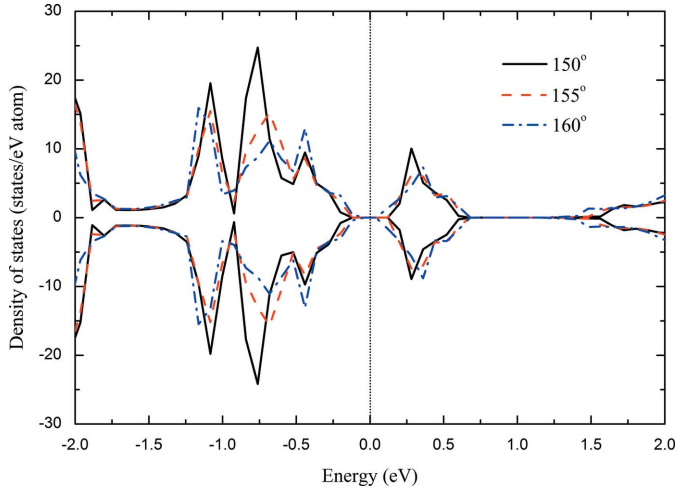

Figure 6
Total densities of states with variation in the Ir—O1—Ir angle θ.

Summarizing, for the Ir-vacant $Sr_2Ir_{1-x}O_4$ system the Ir-vacancies finely modulate the local atomic structure, *i.e.* the topology of IrO_6 octahedra and the Ir—O1—Ir bond angle. The cooperative contributions of distorted IrO_6 octahedra and the decreased Ir—O1—Ir angle lead to an increment of the band gap between LHB and UHB states, and account for an enhanced insulating behavior in $Sr_2Ir_{1-x}O_4$ compounds.

4. Conclusion

We investigated the Ir-vacancies effect on the Ir valence state and local atomic structure of the $Sr_2Ir_{1-x}O_4$ system revealed by Ir $L_{2,3}$-edge XAS. First of all, a mixed population of Ir^{4+} and Ir^{5+} ions was observed in Ir-vacant compounds from both Ir L_2- and L_3-edge XANES spectra. Thus the holes are barely doped into the $Sr_2Ir_{1-x}O_4$ system. Structurally, with the presence of Ir-vacancies, the IrO_6 octahedra became more distorted, and the in-plane Ir—O1—Ir bond angle decreased from 159.0 (3)° to 154.8 (3)°. Combined with the DFT calculations, we found that both the distorted IrO_6 octahedra and the decreased Ir—O1—Ir angle contributed to an enhanced insulating behavior in the $Sr_2Ir_{1-x}O_4$ system.

Funding information

This work was partly supported by the National Natural Science Foundation of China (NSFC 11405089, 11504182 and U1732126), the General Program of Natural Science Foundation of Jiangsu Province of China (No. BK20171440), Jiangsu Natural Science Foundation for Excellent Young Scholar (BK20170101), the 'Six Talents Peak' Foundation of Jiangsu Province (2014-XCL-015) and the Natural Science Foundation of Nanjing University of Posts and Telecommunications (NY218039).

References

Ankudinov, A. L., Ravel, B., Rehr, J. J. & Conradson, S. D. (1998). *Phys. Rev. B*, **58**, 7565–7576.
Bednorz, J. G. & Müller, K. A. (1986). *Z. Phys. B Condens. Matter*, **64**, 189–193.
Cao, G., Terzic, J., Zhao, H. D., Zheng, H., De Long, L. E. & Riseborough, P. S. (2018). *Phys. Rev. Lett.* **120**, 017201.
Cheng, J., Sun, X. Y., Liu, S. L., Li, B., Wang, H. Y., Dong, P., Wang, Y. & Xu, W. (2016). *New J. Phys.* **18**, 093019.
Cheng, J., Zhu, C. M., Liu, S. L., Li, B., Wang, H. Y., Wang, Y. & Xu, W. (2017). *Mater. Res. Bull.* **90**, 1.
Chikara, S., Fabbris, G., Terzic, J., Cao, G., Khomskii, D. & Haskel, D. (2017). *Phys. Rev. B*, **95**, 060407.
Chikara, S., Korneta, O., Crummett, W. P., DeLong, L. E., Schlottmann, P. & Cao, G. (2009). *Phys. Rev. B*, **80**, 140407.
Clancy, J. P., Chen, N., Kim, C. Y., Chen, W. F., Plumb, K. W., Jeon, B. C., Noh, T. W. & Kim, Y. J. (2012). *Phys. Rev. B*, **86**, 195131.
Crawford, M. K., Subramanian, M. A., Harlow, R. L., Fernandez-Baca, J. A., Wang, Z. R. & Johnston, D. C. (1994). *Phys. Rev. B*, **49**, 9198–9201.
Ge, M., Qi, T. F., Korneta, O. B., De Long, D. E., Schlottmann, P., Crummett, W. P. & Cao, G. (2011). *Phys. Rev. B*, **84**, 100402.
Granado, E., Mendonça-Ferreira, L., Garcia, F., Azevedo, G. de M., Fabbris, G., Bittar, E. M., Adriano, C., Garitezi, T. M., Rosa, P. F. S., Bufaiçal, L. F., Avila, M. A., Terashita, H. & Pagliuso, P. G. (2011). *Phys. Rev. B*, **83**, 184508.
Kim, B. J., Jin, H., Moon, S. J., Kim, J. Y., Park, B. G., Leem, C. S., Yu, J., Noh, T. W., Kim, C., Oh, S. J., Park, J. H., Durairaj, V., Cao, G. & Rotenberg, E. (2008). *Phys. Rev. Lett.* **101**, 076402.
Kim, B. J., Ohsumi, H., Komesu, T., Sakai, S., Morita, T., Takagi, H. & Arima, T. (2009). *Science*, **323**, 1329–1332.
Kim, J., Casa, D., Upton, M. H., Gog, T., Kim, Y. J., Mitchell, J. F., van Veenendaal, M., Daghofer, M., van den Brink, J., Khaliullin, G. & Kim, B. J. (2012). *Phys. Rev. Lett.* **108**, 177003.
Kim, Y. K., Sung, N. H., Denlinger, J. D. & Kim, B. J. (2016). *Nat. Phys.* **12**, 37–41.
Klein, Y. & Terasaki, I. (2008). *J. Phys. Condens. Matter*, **20**, 295201.
Kong, J. M., Liu, S. L., Cheng, J., Wang, H. Y., Li, X.-A. & Wang, Z. H. (2015). *Solid State Commun.* **220**, 39–44.
Korneta, O. B., Qi, T. F., Chikara, S., Parkin, S., De Long, L. E., Schlottmann, P. & Cao, G. (2010). *Phys. Rev. B*, **82**, 115117.
Meng, Z. Y., Kim, Y. B. & Kee, H. Y. (2014). *Phys. Rev. Lett.* **113**, 177003.
Nakatsuji, S. & Maeno, Y. (2000). *Phys. Rev. Lett.* **84**, 2666–2669.
Nelson, K. D., Mao, Z. Q., Maeno, Y. & Liu, Y. (2004). *Science*, **306**, 1151–1154.
Newville, M. (2001). *J. Synchrotron Rad.* **8**, 322–324.
Ozaki, T. (2003). *Phys. Rev. B*, **67**, 155108.
Rehr, J. J. & Albers, R. C. (2000). *Rev. Mod. Phys.* **72**, 621–654.
Sun, X. Y., Liu, S. L., Wang, H. Y., Li, B., Cheng, J. & Wang, Z. H. (2016). *J. Alloys Compd.* **687**, 712–719.
Watanabe, H., Shirakawa, T. & Yunoki, S. (2013). *Phys. Rev. Lett.* **110**, 027002.
Witczak-Krempa, W., Chen, G., Kim, Y. B. & Balents, L. (2014). *Annu. Rev. Condens. Matter Phys.* **5**, 57–82.
Yan, Y. J., Ren, M. Q., Xu, H. C., Xie, B. P., Tao, R., Choi, H. Y., Lee, N., Choi, Y. J., Zhang, T. & Feng, D. L. (2015). *Phys. Rev. X*, **5**, 041018.
Yang, Y., Wang, W. S., Liu, J. G., Chen, H., Dai, J. H. & Wang, Q. H. (2014). *Phys. Rev. B*, **89**, 094518.
Yu, H. T., Liu, S. L., Li, B., Wang, H. Y., Cheng, J. & Wang, Z. H. (2017). *Europhys. Lett.* **120**, 27007.